Coherent Marine Radar Measurements of Ocean Wave Frequency Spectra

Dennis B Trizna
Imaging Science Research, Inc.
6103B Virgo Court
Burke, VA 22015 USA

Abstract- **We have been developed two radars for radial Doppler velocity measurements: a coherent marine radar (COHrad), and a standard marine radar modified to coherent-on-receive capability (CORrad). Both measure the intensity and the radial velocity component of the radar echo. The latter can be used to generate orbital wave velocity spatial maps of ocean waves, as well as the mean radial ocean surface velocity when sequences of map images are summed. These radars allow direct measurement of the ocean wave spectrum by means of 3D-FFT processing of a sequence of coherent radar images of orbital wave spatial patterns (U.S. Patent #8305257). We present results of radar measurements of RMS waveheight for COH and COR radars, using both horizontally and vertically polarized antennas. Vertical polarization is found to mitigate against errors in rms wave height retrieval for high wave conditions, when accelerating breaking features generate errors for horizontal polarization. Results are presented of time series of 16 frequency components of omni-directional spectra and compared with data from a pressure sensor array at the U.S. Army Field Research Facility in Duck, NC.**

I. OMEGA-K SPECTRA

Marine radars offer a snapshot image sequence each 1.25 or 2.5 s of the coastal wave field that can be used for the application of various image processing algorithms. A number of researchers have established the utility of using both radar and optical video image sequences to derive useful coastal ocean properties from such data [1-6]. We have recently developed an integrated radar and data acqusition package to make such measurements synoptically and unattended. The prototype system has been set up at the U.S. Army Corps of Engineers Field Research Facility (FRF), Duck, NC for extensive testing and ground truth comparison. Results from that site are presented here.

II. COHERENT RADAR DESCRIPTION

The Sitex radar pedestal is used for both ISR radar systems, an example of which is show below in Fig. 1.

Figure. 1. ISR coherent marine radar used for wave sensing.

The radars used for the results presented here are two . The first is our coherent-on-receive ISR CORrad Digital Imaging Radar Model 12.8, based on a modified Koden 12-kWatt 8' antenna system, with our digital acquisition system and signal processing systems, Radar Image Processing Suite (RIPS). The second is a fully coherent radar (COHrad) using a new solid state transceiver.

COHrad makes use of pulse compression to achieve improved gain, equivalent to the standard marine radar, allowing it to operate with just 5-watts peak power. A 1-µs transmitted pulse is shown in Fig. 2a below, chirped over 30 MHz, and mixed up to X-band for transmission. Echoes have a similar shape and pulse compression correlation creates in-phase (I) and quadrature (Q) samples that are used for velocity measures. These are shown in Fig. 2b and 2c below.

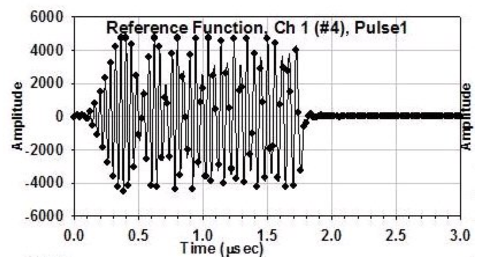

Figure 2a. Chirped pulse transmitted, after mixing to X-band.

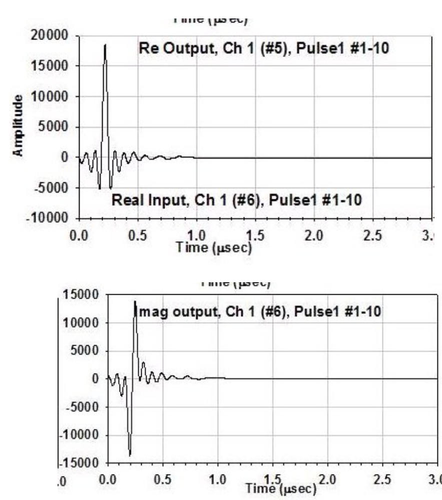

Figure 2b-c. Compressed I,Q pair signals

978-0-933957-43-5 ©2015 MTS

The phase at each time sample is determined from the equation ATAN(I/Q), and a phase difference, dϕ, from two consecutive pulses is calculated for each range sample. This is proportional to the radial velocity using the Doppler equation, v = dϕ * (λ/2)*PRF/2, PRF being Pulse-Repetition-Frequency. The range-azimuth radial velocities are then transformed into Cartesian co-ordinates for each rotation of the radar. The radar video echo intensity signal, S(R.ϕ), is calculated at each pixel for comparison using $S(R.\phi) = (I^2+Q^2)^{1/2}$. A map of images of intensity and radial velocity is shown below in Fig. 3a and 3b.

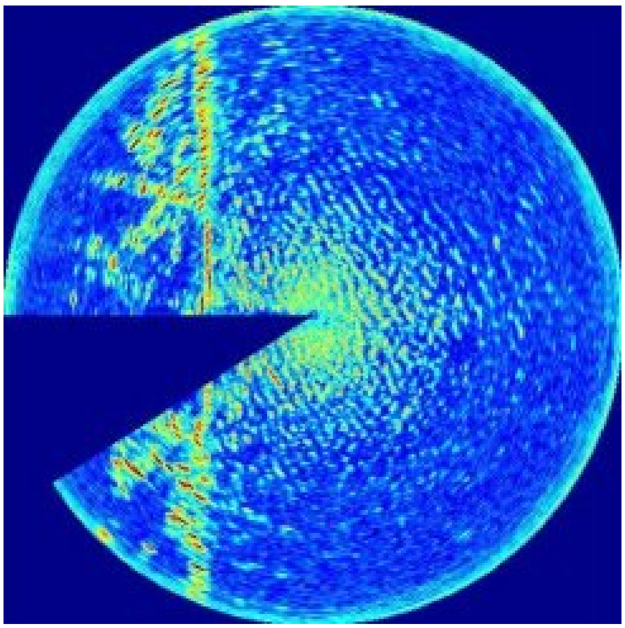

Figure 3a. COHrad echo intensity image.

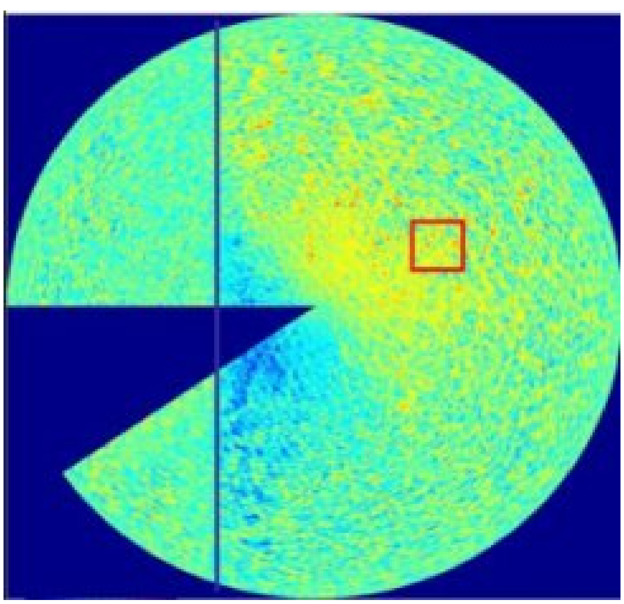

Figure 3b. COHrad radial velocity image.

The radial velocity map appears to show usable information at ranges where the intensity signal is weak, but stil provides sufficient quality I/Q values to allow phases to be determined. There is an offset due to current here that will be discussed later. The red box represents a user-selectable 64x64 sqaure of pixels that can be arbitrarilty located for successive rotations and used as input to a 3D-FFT analysis. This outupt is used to determined spectral samples of waveheight-squared/Hz. The location of this window can be moved about the radar coverage scene to study wave dissipation is space, for example, or wave refraction spectra in unusual bathymetry environments. One must correct for the radar aspect relative to the primary wave direction, as the radar radial component will vary like cosine of the difference of wave travel vs radar illumination.

III. OMEGA-K SPECTRA

Fig. 4 represents a subset of 6 frequency spectra from a set of 32 that are available when using 64 rotations of 64x64 pixels, then averaging over 8 of such sets covering a 10-min period. The yellow circle seen represents the shallow water dispersion rule for the depth chosen, 10 m, while the red circle represents deep water.

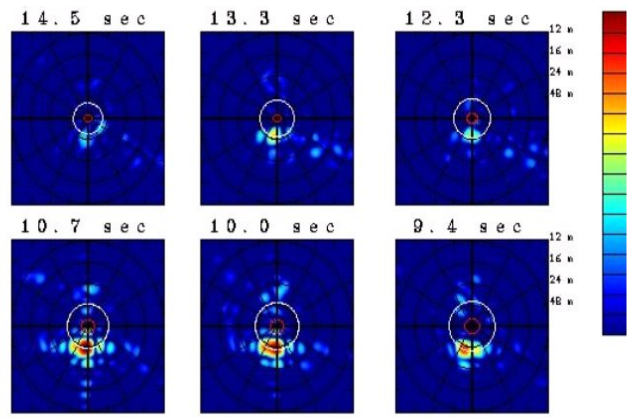

Figure. 4. K_x-K_y Spectra at each of a series of wave frequencies from the Ω-K spectral analysis.

The spectral peaks clearly lie on the shallow water dispersion circle chosen, and each image can be filtered using a band between, say, 80% and 120% of this radius, to account for tidal changes in depth that moves the peaks radially. All energy in this band will represent samples of wave height squared per unit Hz, (0.4Hz/64 in this case). This is obtained by relating the radial velocity, V_{rad}, to the spectral waveheight component, using the time derivative of the equation defining the x-position of a patch of water on a wave surface :

$$X(t) = (H/2) \sin(kx+\Omega t) \quad (1)$$

$$V_{rad} = dX(t)/dt = (H/2)\, \Omega \cos(kx + \Omega t) \quad (2)$$

In the case of processing the intensity image of a standard marine radar, similar image intensity spectra result, but each radar frequency component must be scaled to some surface truth representation of the weave frequency spectrum using an emprical constant, a spectral Modulation Transfer Function. This has shown to be in error when environental conditions change (wind direction relative to wave direction, for example), and if the radar modulator ages with time and exhibits chaning output power. The coherent radar approach requires no such scaling, and is independent of such environmental factors. A patent based on this approach has been applice for by ISR and is pending, and an international provisional patent has also been filed.

IV. FREQUENCY SPECTRA AND H_m0

If one sums the spectral energy in the band about the shallow water dispersion relation for each of 32 windows, one derives an omni-directional freqeuency spectrum. A comparison of that derived from coherent radar data over 10 minutes, and the pressure array sensor at the FRF for two overlapping periods of 3-hr each is shown in Fig. 5 below.

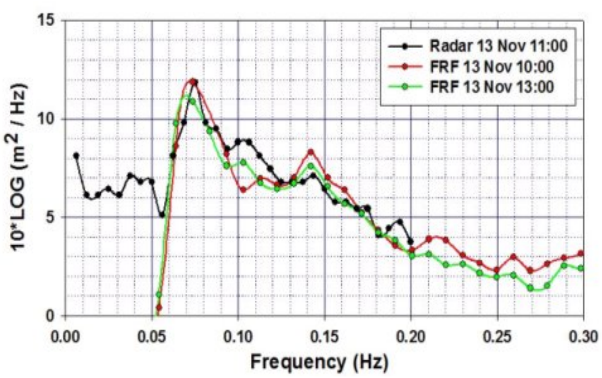

Figure 5. Frequency spectra from COHrad and pressure array.

If one sums the energy from each spectral peak in the frequency spectrum above, one forms H_m0, a RMS waveheight estimate. During November of 2009, Hurricane Ida passed offshore of the FRF site and waves of 4-m were observed. Below are plotted the time series of H_m0 from the radar vs that from the FRF pressure sensor array.

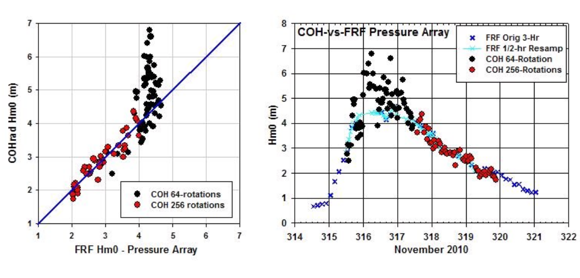

Figure 6. Hm0 time series from radar vs FRF pressure array.

The black circles represent a subset of data during which strong wave breaking occured in the analysis sqare, and subsided as the square was rotated in angle nortth of shore normal in comparison analyses. Strong breaking crests are thus illuminated so that specular scatter from crest features are less apt to scatter back to the radar when not illuminated normal to their linear edge. Non-breaking wave conditions offshore are represented by the red circles. The agreement is quite good for these conditions and this case of illumination into incoming waves offshore of the pier end. A vertically polarized antenna is known to be less affected by breaking wave features, but one was not available for use then.

The CORrad was run simultaneously from the same location a frew meters away and processing that data in a similar fashion produced results for Hm0 as well. These are shown in Fig. 8 below.

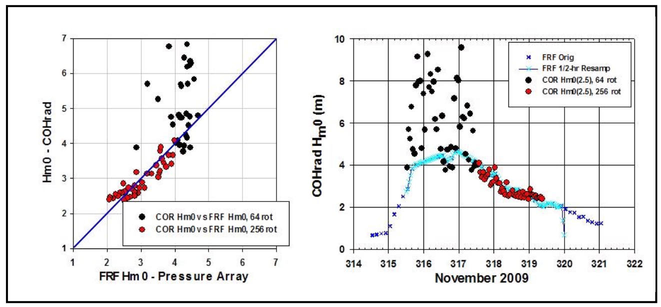

Figure 7. CORrad Hm0 vs FRF pressure array results

The results from the CORrad system are quite similar to those of the COHrad for the same period, and the need for more than 64 rotations of data are apparent here as well.

A second experiment was conducted in 2010, from a location on shore instead of the end of the FRF pier. This was data from a CORrad also, running over 512 rotations at twice the rotation rate of the COHrad, so covering the same 10-min or so time period. The height of the antenna was lower than that at the end of the pier, atop a 32' telescoping tower on ~3-m mean height behind the dune at the FRF site. They were collected at relatively short range, 384 m offshore, as only 512 range samples were collected, and compared with FRF data from ~800 m offshore.

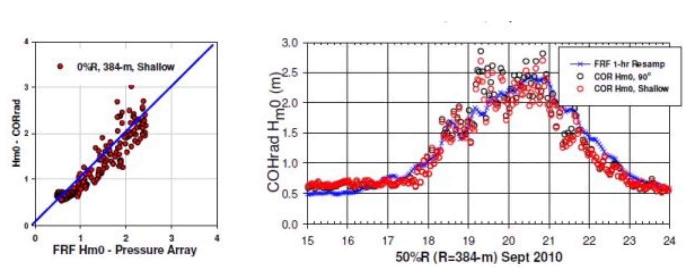

Figure 8. CORrad data from a shore site.

V. V-POL: HURRICANE IRENE H_m0

In the summer of 2011, Hurricane Irene passed the Outer Banks inland of our radar site, but waves generated earlier while the storm was still offshore generated 4.2 m waves at the FRF pier. In preparation for this storm, the COHrad antenna was switched from a 9' horizontally polarized antenna to a 4' vertically polarized unit. The hypothesis to explain the outliers seen in the previous figures was that for very high waves, severe spilling breakers were occurring in far deeper water than under lower wave conditions, and the acceleration of wave breaking crests under such conditions might be biasing the radial velocity measurements made with horizontal polarization. In a previous work [8], we showed the dramatic difference between low grazing angle images for HH and VV polarization. For HH, small scale breaking features dominate the scene, with their azimuthal echo strength dependence falling off when illuminated further off normal to the breaking edge. This behavior suggested a scattering width of about 25 cm for the small pancake breakers that were observed visually, with virtually no echo when seen from a direction illuminating the back of these waves, opposite the wind. For VV, these discrete echoes do not appear, and distributed Bragg sources dominate the scattering process, with a modest front-to-back ratio of 6 dB or so when looking into the wind versus opposite it. This suggests that a vertically polarized antenna might eliminate outliers due to breaking wave crests of a much larger scale than observed in [8].

Figure 9 shows a time series of H_m0 measured using COHrad with the V-pol antenna for wave conditions up to 4.2 m. H_m0 outliers seen previously are not seen here, for even higher seas than then.

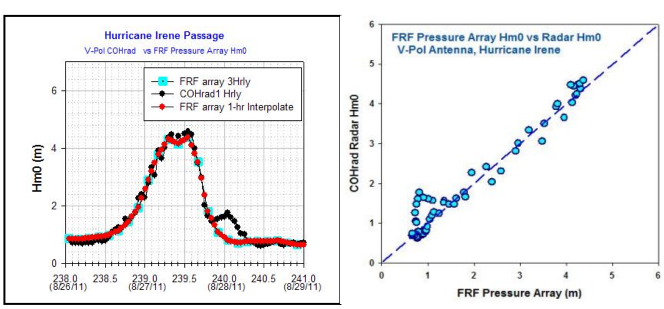

Figure 9. COHrad data during Irene with a V-pol antenna.

For the same time, a CORrad was run with an H-pol antenna, covering the same period of collection and location at the end of the FRF pier. There were outliers in these data, starting at about the same H_m0 value as in figures 7 and 8 above. Thus, we feel that our hypothesis has been validated, that outliers for high sea states above 3 m using horizontally polarized antennas will generate errors in H_m0 retrieval due to large scale spilling breaker strong scatter for this polarization. However, as small scale breaking allows one to image the location of the offshore bar, as we have shown previously, there may be a trade off in keeping an H-pol antenna for coastal sites, where the very high sea conditions are rarely encountered, but bard imaging is important. We have not yet compared the sensitivity between the two polarizations for very weak wave conditions, where H-pol might provide a reasonable echo for other applications as well. The agreement for the 0.4-m minima seen in Figure 7 do suggest that the ability to retrieve wave spectra for small waves is not hampered severely.

VI. FREQUENCY SPECTRA TIME SERIES

For data discussed in Fig. 8, a more detailed comparison was made of each component of the frequency spectrum similar to the single one in Fig. 5 above. A time series of measurements is shown in Fig. 10 below, for a subset of 8 of 32 frequencies available.

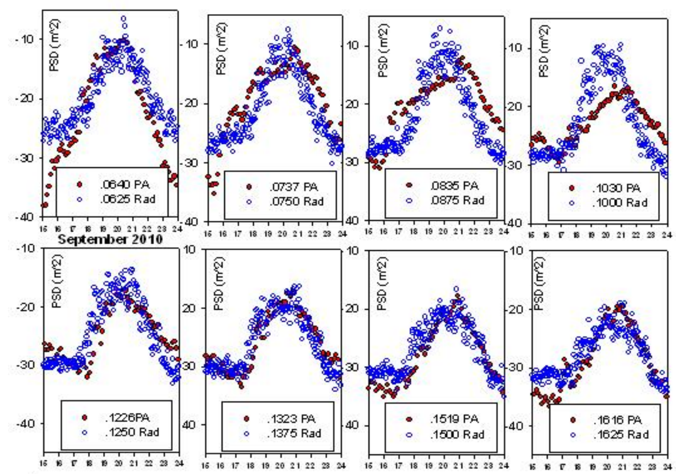

Figure 10. Time series of spectral components from radar (blue) and FRF Pressure Sensor Array (red)

The pressure sensor data is plotted in 3 hour increments using a 3-hr analysis, while the radar data is hourly using just ten minutes of data. Scatter diagram comparisons are not available until re-sampling of the PSA data is done, both in time and frequency. Nearest neighbor frequencies were used in these plots. It appears that the PA data for the 0.1030 Hz frequency component shifts to the 21^{st} of September, compared to other PSA frequencies. The radar results peak all at a similar time on about September 20^{th}.

VII. SUMMARY

We have demonstrated the use of a newly designed coherent marine radar to measure directional wave spectra and surface radial currents. Data were compared with surface truth instrumentation from the USACE Field Research Facility, both pressure array sensor data for wave height, and AWAC acoustic sensors for currents. Data from a coherent-on-receive radar that was run simultaneousl from the end of the pier at the FRF and compared favorably as well. For this location, currents along shore can be measured reasonably accurately for the modest radar height of roughly 11 m, as the radar is looking along the crests and troughs and does not suffer shadowing, even for modest to low radar height for this geometry. Looking offshore, the troughs would be shadowed by the crests for very steep waves, and the orbital wave velocity would not present a zero mean to the radar look. We found this to be the case for a shore based radar on another occasion, where the currents were in error due to crest orbital wave influences. For this case, the wave height analysis was still quite respectable. On more recent observations at other sites with radar heights ranging from 19 m to 26 m, no shadowing was encountered and long range currents could be measured accurately.

Results from a veretically polarized antenna were also presented that eliminated the high outlyier H_m0 values seen in earlier experiments using horizontally polarized antennas. These results confirmed previous observations of small scale breaking effects on horizontally polarized scatter from small scale breaking features. Accerating large scale breaking crest features contribute anomolous high Doppler shifts that do not reflect the orbital wave motion of the underlying linear wave. As a result of this experiment, ISR constructs V-pol antennas for ocean wave H_m0 retrieval applications. These antennas probably provide a more meaningful surface velocity measure as they would elimiate small scale breaking accelerations that could contaminate mean velocities

ACKNOLEDGEMENTS

We wish to acknowledge the data provided by the USACE FRF, in particular, to Kent Hathaway who extracted the data from historical records that allowed the comparisons to be made on a timely basis. ISR has a continuing Co-operative R&D Agreement with the FRF.

REFERENCES

[1] Dankert, H., J. Horstmann, and W. Rosenthal, Ocean Wind Fields Retrieved from Radar-Image Sequences, J. Geophys. Res.. Vol. 108, 2005.

[2] Young, I.R., W. Rosenthal, F. Ziemer, A three-dimensional analysis of marine radar images for the determination of ocean wave directionality and surface currents, JGR, **90**, C1, pp. 1049-1059, 1985.

[3] Trizna, D.B., "Errors in Bathymetric Retrievals using Linear Dispersion In 3D FFT Analysis of Marine Radar Ocean Wave Imagery," IEEE Trans. Geosciences and Remote Sensing, **39**, pp. 2465-2469, 2001.

[4] C.M. Senet, J. Seemann, F. Ziemer, An iterative technique to determine the near surface current velocity from time series of sea surface images, Oceans '97, Halifax, 1997.

[5] Dugan, J.P., H.H. Suzukawa, C.P. Forsythe, M.S. Farber, Ocean wave dispersions surface measured with airborne IR imaging system, IEEE Trans. Geosciences and Remote Sensing, **34**, pp. 1282-1284, 1996.

[6] Dugan, J.P., C.P. Forsythe, H.H. Suzukawa, M.S. Farber, Bathymetry estimates from long range airborne imaging systems, Proc. 4th Int. Conf. On Remote Sensing for Marine and Coastal Environments, Orlando FL, 1997.

[7] Stockdon, H.F., and R.A. Holman, Estimation of wave phase speed and nearshore bathymetry from video imagery, J. Geophysical Res., **105**, pp. 22,015-22,034, 2000.

[8] Trizna, D. B., Coherent Marine Radar Measurements of Ocean Surface Currents and Directional Spectra, Oceans 2011 Santander, 6-10 June 2011.

[9] Trizna, D.B., Carlson., D.J., Studies of Dual Polarized Low Grazing Angle Radar Sea Scatter in Nearshore Regions, IEEE Trans. On Geoscience and Remote Sensing, Vol 34, pp 747-757.